Available online at www.sciencedirect.com
SCIENCE DIRECT®
International Journal of Heat and Mass Transfer 47 (2004) 215–227
International Journal of HEAT and MASS TRANSFER
www.elsevier.com/locate/ijhmt

Joule heating effect on electroosmotic flow and mass species transport in a microcapillary

G.Y. Tang, C. Yang *, J.C. Chai, H.Q. Gong

School of Mechanical and Production Engineering, Nanyang Technological University, North Spine (N3), Level 2 Nanyang Avenue, Singapore 639798, Singapore

Received 13 December 2002; received in revised form 28 July 2003

Abstract

This study presents a numerical analysis of Joule heating effect on the electroosmotic flow and mass species transport, which has a direct application in the capillary electrophoresis based BioChip technology. A rigorous mathematic model for describing the Joule heating in an electroosmotic flow including the Poisson–Boltzmann equation, the modified Navier–Stokes equations and the energy equation is developed. All these equations are coupled through the temperature-dependent liquid dielectric constant, viscosity, and thermal conductivity. By numerically solving the aforementioned equations simultaneously, the double layer potential profile, the electroosmotic flow field, and the temperature distribution in a cylindrical microcapillary are computed. A systematic study is carried out to evaluate the Joule heating and its effects under the influences of the capillary radius, the buffer solution concentration, the applied electric field strength, and the heat transfer coefficient. In addition, the Joule heating effect on sample species transport in a microcapillary is also investigated by numerically solving the mass transfer equation with consideration of temperature-dependent diffusion coefficient and electrophoresis mobility. The simulations reveal that the presence of the Joule heating could have a great impact on the electroosmotic flow and mass species transport.

Keywords: Joule heating; Electroosmotic flow; Electrokinetic mass transport

1. Introduction

Electroosmosis refers to liquid flow induced by an applied external electric field along electrostatically charged surfaces. It is one of the basic electrokinetic phenomena and has been found a variety of practical applications such as dewatering of waste sludge and removing heavy metal ions from soils for environmental remediation [1]. During recent years, due to the rapid development of Lab-on-a-chip (or Biochip) technology, the electroosmosis is being utilized extensively as the driving forces to manipulate liquid flows such as pumping, valving, mixing, splitting etc., and to transport and control liquid samples of nanovolumes in micro-fluidic devices used for chemical and biological analysis and medical diagnosis [2,3].

In the literature, a great deal of information has been generated on electroosmotic flow in microcapillaries of various geometric domains such as slit parallel plate [4], cylindrical capillary [5,6], annulus [7], elliptical pore [8], rectangular microchannel [9], and T and Y microchannel structures [10]. Noticing that above mentioned studies of electroosmotic flow focus on fully developed status only, Yang et al. [11] simultaneously solved the coupled Poisson equation, Nernst–Planck equation, and full Navier–Stokes (N–S) equation to study the time and space development of electroosmotic flow in a two-parallel plate microchannel. Recently, Santiago [12] analyzed the effects of fluid inertia and pressure on the velocity and vorticity fields of an electroosmotic flow.

However, all aforementioned studies assume a negligible effect of Joule heating on electroosmotic flow. It is well known that the so-called Joule heating is generated

* Corresponding author. Tel.: +65-6790-4883; fax: +65-6791-1859.
E-mail address: mcyang@ntu.edu.sg (C. Yang).

0017-9310/$ - see front matter © 2003 Elsevier Ltd. All rights reserved.
doi:10.1016/j.ijheatmasstransfer.2003.07.006

Nomenclature

C	ionic concentration of the electrolyte (M)
C_i	mass concentration of the ith species (M)
c_p	specific heat capacity of the electrolyte ($J\,kg^{-1}\,K^{-1}$)
$D_i(T)$	diffusion coefficient of the ith species ($m^2\,s^{-1}$)
E	strength of the applied electric field ($V\,m^{-1}$)
e	fundamental charge (1.602×10^{-19} C)
h	heat transfer coefficient ($W\,m^{-2}\,K^{-1}$)
I	electrical current density ($A\,m^{-2}$)
k_b	Boltzmann constant (1.38×10^{-23} $J\,K^{-1}$)
$k_l(T)$	thermal conductivity of the electrolyte solution ($W\,m^{-1}\,K^{-1}$)
k_s	thermal conductivity of the capillary wall ($W\,m^{-1}\,K^{-1}$)
L	capillary channel length (m)
n_+, n_-	local number concentration of cations and anions, respectively (m^{-3})
n_0	bulk number concentration of ions in the electrolyte solution (m^{-3})
Pr	Prandtl number
$\dot{q}$	Joule heat generation ($W\,m^{-3}$)
r	coordinate in radial direction
R	radius of the capillary (m)
Re	Reynolds number
Sc	Schmidt number
t	time (s)
T	temperature (K)
T_0	surrounding temperature (K)
U_s	Smoluchowski velocity ($m\,s^{-1}$)
u_{zi}, u_{ri}	electrophoretic velocity of the ith species in axial and radial direction, respectively ($m\,s^{-1}$)
v_z, v_r	electroosmotic flow velocity in axial and radial direction, respectively ($m\,s^{-1}$)
z	coordinate in axial direction

Greek symbols

α	thermal diffusivity ($m^2\,s^{-1}$)
ε_0	permittivity of vacuum (8.85×10^{-12} $C\,V^{-1}\,m^{-1}$)
$\varepsilon(T)$	relative dielectric constant of the electrolyte
ζ	zeta potential of the capillary wall (V)
η_+, η_-	the number of moles of cation and anion in the electrolyte, respectively (M)
κ	Debye–Hückel parameter (m^{-1})
λ	electrical conductivity of the electrolyte solution ($S\,m^{-1}$)
λ_+, λ_-	equivalent ionic conductivity of the cations and anions, respectively ($m^2\,S\,mol^{-1}$)
$\mu(T)$	viscosity of the electrolyte solution (Pa s)
σ	valence of the ions of the electrolyte solution
ρ	density of the electrolyte solution ($kg\,m^{-3}$)
ρ_e	local net electrical charge density in the electrolyte solution ($C\,m^{-3}$)
Φ	thermal viscous dissipation ($W\,m^{-3}$)
ψ	local electrical potential (V)

Subscript

ref	reference parameters

when an electric field is applied across conductive liquids. Such Joule heating not only can cause temperature increase but also may create temperature gradient. The change of liquid temperature and the presence of temperature gradient would have an impact on the electroosmotic flow and bio-sample transport and separation. Previous studies [13–20] have amply demonstrated that the effects of Joule heating can result in low column separation efficiency, reduction of analysis resolution, and even loss of injected samples. In addition, temperature rise can lead to the decomposition of thermally labile samples and the formation of gas bubbles.

Theoretical and experimental studies of the Joule heating and its effects on sample separation have been reported in the literature. Simplified theoretical analyses were conducted to obtain analytical expressions for the effect of the Joule heating on buffer solution mean temperature, electroosmotic velocity and electrophoretic mobility. Knox and McCormack [13,14] used three different methods to calculate the mean temperature change due to Joule heating. Grushka et al. [15] examined the effect of temperature difference on the efficiency of the capillary zone electrophoresis using a parabolic temperature distribution assumption. Jones and Grushka [16] used a simplified one-dimensional model to verify that the parabolic temperature profile is valid for low input powers, but the parabolic profile is distorted for high input powers. Recently, Bosse and Arce [17,18] carried out systematic studies of Joule heating effect on dispersive mixing in electrophoretic cells, focusing on both hydrodynamic and convective-diffusive transport aspects. However, their analysis is only limited to electrophoretic cells where the two ends of the cell are closed. Furthermore, their models do not include electroosmotic flow.

Many experimental studies of Joule heating in the capillary electrophoresis (CE) have been report since Knox and McCormack [13]. Swinney and Bornhop [19] measured the Joule heating in a chip-scale CE by using a

novel picoliter volume interferometer. Their results showed that the Joule heating effects on chip-based CE have been underestimated and hence there is a need to readdress the theoretical model. Gobie and Ivory [20] proposed a method to compensate sample's electrophoretic velocity distortion by inducing an opposing Poiseuille flow. As a result, the sample velocity exhibits a nearly flat profile, and a good improvement was observed.

Nonetheless, previous model developments are either empirical or based on simplified theories, and hence they cannot provide detailed information about the nature of the Joule heating in CE processes. Further, based on available experimental techniques, only averaged-data for temperature and sample concentration can be obtained. This study therefore attempts to increase our understanding of the thermal aspects of electroosmotic flow and electrophoresis so as to achieve a better design and process control of the CE. To our best knowledge, this is the first to provide an in-depth analysis of the Joule heating and its effects on the electroosmotic flow and sample transport based on rigorous mathematical models. The structure of the paper is organized as follow: First, the problem of Joule heating in CE is formed, and theoretical models are developed to include the Poisson–Boltzmann (P–B) equation, equation of motion, and energy equation for describing the electrical potential profile, electroosmotic flow field, and temperature distribution due to Joule heating, respectively. All the three equations are coupled by taking into account of temperature-dependent thermophysical properties. Then, the model of sample species transport in the capillary is also formulated. The mathematical models are numerically solved using a finite-volume based CFD technique. Computations for double layer potential, velocity, temperature and sample concentration distributions in a microcapillary are performed under influences of the radius of capillary, the concentration of electrolyte solution, the strength of applied electrical field, and the heat transfer coefficient outside capillary wall.

2. Problem formulation

In electroosmotic flow, the motion of the fluid is mainly caused by an applied electric field. No external pressure difference between the inlet and outlet reservoirs is imposed. The model developed in this study includes the P–B equation governing the electrical potential distribution, the modified N–S equations describing the motion of liquid driven by electrokinetic body forces, and the energy equation governing the temperature field due to Joule heating. Since liquid properties including the dielectric constant, the liquid viscosity, and the liquid thermal conductivity are temperature dependent, the P–B equation, the N–S equations, and the energy equation are strongly coupled. Moreover, in view of the fact that electroosmotic flow is mainly used for delivering and separating chemical or biological samples, the mass species transport equation is therefore included into the model development to examine the Joule heating effect. In addition, the computational domain in the present work is chosen as a cylindrical microcapillary, which is widely used in several bioengineering processes such as CE and high-performance liquid chromatography.

2.1. The Poisson–Boltzmann equation

Consider an electroosmotic flow in a cylindrical microcapillary of an inner radius, R and a length, L as shown in Fig. 1. When a solid surface is in contact with a polar medium, the surface usually becomes charged [21]. Due to electrostatic interactions, both co-ions and counter-ions are preferentially redistributed near the charged surface, leading to the formation of an electrical double layer (EDL). According to the theory of electrostatics, the electrical potential distribution, $\psi(r,z)$ is governed by the Poisson equation [1,21],

$$\frac{1}{r}\frac{\partial}{\partial r}\left[r\varepsilon(T)\frac{\partial\psi}{\partial r}\right]+\frac{\partial}{\partial z}\left[\varepsilon(T)\frac{\partial\psi}{\partial z}\right]=-\frac{\rho_e}{\varepsilon_0} \tag{1}$$

where $\varepsilon(T)$ is the dielectric constant of the electrolyte and is considered as a function of temperature, expressed by $\varepsilon(T)=305.7\exp\left(-\frac{T}{219}\right)$. In this study, the ionic concentration distributions for both anions and cations are assumed to follow the Boltzmann distributions [9], and for a symmetric electrolyte (i.e., the co-ions and counter-ions have same charge valence, $|\sigma_+|=|\sigma_-|=\sigma$), they can be written as [9],

$$n_+=n_0e^{-\sigma e\psi/k_bT}\quad n_+=n_0e^{\sigma e\psi/k_bT} \tag{2}$$

Then the local charge density, ρ_e is given by

$$\rho_e(r,z)=\sigma e(n_+-n_-)=-2\sigma en_0\sinh\left(\frac{\sigma e\psi}{k_bT}\right) \tag{3}$$

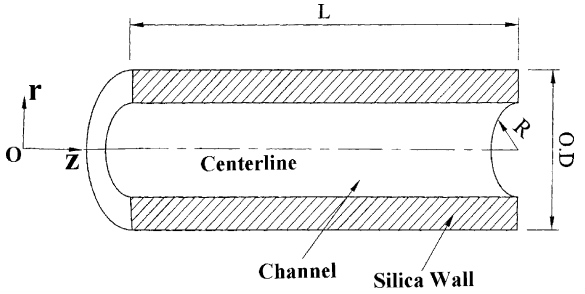

Fig. 1. Schematic diagram of the circular microcapillary.

Combining Eqs. (1) and (3), we can obtain the P–B equation

$$\frac{1}{r}\frac{\partial}{\partial r}\left[r\varepsilon(T)\frac{\partial\psi}{\partial r}\right]+\frac{\partial}{\partial z}\left[\varepsilon(T)\frac{\partial\psi}{\partial z}\right]=\frac{2\sigma e n_0}{\varepsilon_0}\sinh\left(\frac{e\psi}{k_{\mathrm{b}}T}\right) \tag{4}$$

Introducing the following non-dimensional parameters:

$$\bar{r}=\frac{r}{R}\quad \bar{z}=\frac{z}{R}\quad \bar{\psi}=\frac{\sigma e\psi}{k_{\mathrm{b}}T}\quad \bar{\varepsilon}=\frac{\varepsilon(T)}{\varepsilon_{\mathrm{ref}}} \tag{5}$$

Eq. (4) can be further expressed in dimensionless form as,

$$\frac{1}{\bar{r}}\frac{\partial}{\partial\bar{r}}\left[\bar{r}\bar{\varepsilon}\frac{\partial\bar{\psi}}{\partial\bar{r}}\right]+\frac{\partial}{\partial\bar{z}}\left[\bar{\varepsilon}\frac{\partial\bar{\psi}}{\partial\bar{z}}\right]=\frac{2R^2\sigma^2e^2n_0}{\varepsilon_{\mathrm{ref}}\varepsilon_0k_{\mathrm{b}}T}\sinh(\bar{\psi})=(\kappa R)^2\sinh(\bar{\psi}) \tag{6}$$

where $\varepsilon_{\mathrm{ref}}$ is dielectric constant of the solution at room temperature (i.e., $T_{\mathrm{ref}}=20$ °C), and it is chosen to be 80 in all the computation unless specified otherwise. $\kappa=\left(\frac{2n_0\sigma^2e^2}{\varepsilon_{\mathrm{ref}}\varepsilon_0k_{\mathrm{b}}T}\right)^{1/2}$ is the Debye–Hückel parameter, and its reciprocal represents the EDL thickness. In the literature, κR is called the electrokinetic radius. It characterizes the ratio of the geometric dimension to the EDL thickness, and hence denotes the relative contribution of the EDL effect.

2.2. The modified Navier–Stokes equations and energy equation

Different from the conventional pressure-driven flows, the driving force of the electroosmotic flow is due to the interaction between the net charge density in the EDL and the applied electric field. Therefore, the continuity and momentum equations describing a laminar, incompressible, steady flow of an electrolyte solution with temperature-dependent viscosity are modified to [1]

$$\frac{1}{r}\frac{\partial}{\partial r}(rv_r)+\frac{\partial v_z}{\partial z}=0 \tag{7}$$

$$\rho\left[v_r\frac{\partial v_z}{\partial r}+v_z\frac{\partial v_z}{\partial z}\right]=-\frac{\partial p}{\partial z}+\frac{1}{r}\frac{\partial}{\partial r}\left[r\mu(T)\frac{\partial v_z}{\partial r}\right]+\frac{\partial}{\partial z}\left[\mu(T)\frac{\partial v_z}{\partial z}\right]+\rho_{\mathrm{e}}E \tag{8a}$$

$$\rho\left[v_r\frac{\partial v_r}{\partial r}+v_z\frac{\partial v_r}{\partial z}\right]=-\frac{\partial p}{\partial r}+\frac{\partial}{\partial r}\left[\frac{\mu(T)}{r}\frac{\partial(rv_r)}{\partial r}\right]+\frac{\partial}{\partial z}\left[\mu(T)\frac{\partial v_r}{\partial z}\right]-\rho_{\mathrm{e}}\frac{\partial\psi}{\partial r} \tag{8b}$$

where ρ is the density of the electrolyte solution, μ is the viscosity of the electrolyte solution and its dependence of temperature is given by $\mu(T)=2.761\times10^{-6}\exp\left(\frac{1713}{T}\right)$, and E is the strength of an externally applied electric field along the axial direction.

The energy equation taking into account of the temperature-dependent thermal conductivity of the electrolyte solution (expressed by $k_l(T)=0.6+2.5\times10^{-5}T$) can be expressed as

$$\rho c_p\left(v_r\frac{\partial T}{\partial r}+v_z\frac{\partial T}{\partial z}\right)=\frac{1}{r}\frac{\partial}{\partial r}\left[rk_l(T)\frac{\partial T}{\partial r}\right]+\frac{\partial}{\partial z}\left[k_l(T)\frac{\partial T}{\partial z}\right]+\Phi+\dot{q} \tag{9}$$

where c_p is the specific heat capacity of the electrolyte solution. In Eq. (9), the heat source consists of viscous dissipation (Φ) and Joule heating ($\dot{q}$). Heat generation due to viscous dissipation is given as [1]

$$\Phi=2\mu(T)\left[\left(\frac{\partial v_r}{\partial r}\right)^2+\left(\frac{\partial v_z}{\partial z}\right)^2\right]+\mu(T)\left(\frac{\partial v_r}{\partial z}+\frac{\partial v_z}{\partial r}\right)^2 \tag{10}$$

According to the Ohm's law, the heat generation due to Joule heating can be expressed as

$$\dot{q}=\frac{I^2}{\lambda} \tag{11}$$

where I is the electrical current density in the solution and λ is the electrical conductivity of the electrolyte and is given as

$$\lambda=\lambda_+\eta_++\lambda_-\eta_- \tag{12}$$

Here $\lambda_+(T)=\lambda_{+0}+0.025\lambda_{+0}(T-298.13)$ and $\lambda_-(T)=\lambda_{-0}+0.025\lambda_{-0}(T-298.13)$ are ionic conductivity of the cation and anion of the electrolyte, respectively, η_+ and η_- respectively denote the mole concentration of cations and anions of the electrolyte. In this situation, the electrical current density includes two parts, one is due to the applied electric field imposing on the conductive solution ($E\lambda$), the other is due to the net charged density moving with the fluid flow ($v_z\rho_{\mathrm{e}}$). Therefore the electrical current density, I can be further expressed as

$$I=v_z\rho_{\mathrm{e}}+E\lambda \tag{13}$$

Substituting Eqs. (12) and (13) into Eq. (11), we can obtain the following

$$\dot{q}=\frac{(v_z\rho_{\mathrm{e}}+E\lambda)^2}{\lambda} \tag{14}$$

The above governing equations can be non-dimensionalized by introducing the following dimensionless parameters:

$$\bar{v}_z=\frac{v_z}{U_{\mathrm{ref}}}\quad \bar{v}_r=\frac{v_r}{U_{\mathrm{ref}}}\quad \overline{P}=\frac{p}{\rho U_{\mathrm{ref}}^2}\quad \bar{\mu}=\frac{\mu(T)}{\mu_{\mathrm{ref}}} \tag{15a}$$

$$\bar{k}_l = \frac{k_l(T)}{k_{\text{ref}}} \quad \overline{T} = \frac{T - T_{\text{ref}}}{T_0 - T_{\text{ref}}} \quad Re = \frac{\rho R U_{\text{ref}}}{\mu_{\text{ref}}}$$
$$Pr = \frac{\mu_{\text{ref}}}{k_{\text{ref}}/C_p} \tag{15b}$$

where U_{ref}, μ_{ref}, k_{ref}, and T_{ref} are the reference velocity, dynamic viscosity, thermal conductivity, and temperature, respectively, Re is the Reynolds number, and Pr is the Prandtl number. Therefore, Eqs. (7)–(10) and Eq. (14) in dimensionless form are expressed as

$$\frac{1}{\bar{r}}\frac{\partial r}{\partial \bar{r}}(\bar{r}\bar{v}_r) + \frac{\partial \bar{v}_z}{\partial \bar{z}} = 0 \tag{16}$$

$$\bar{v}_r\frac{\partial \bar{v}_z}{\partial \bar{r}} + \bar{v}_z\frac{\partial \bar{v}_z}{\partial \bar{z}} = -\frac{\partial \bar{p}}{\partial \bar{z}} + \frac{1}{Re}\left\{\frac{1}{\bar{r}}\frac{\partial}{\partial \bar{r}}\left[\bar{r}\bar{\mu}\frac{\partial \bar{v}_z}{\partial \bar{r}}\right] + \frac{\partial}{\partial \bar{z}}\left[\bar{\mu}\frac{\partial \bar{v}_z}{\partial \bar{z}}\right]\right\} - A\sinh(\bar{\psi}) \tag{17a}$$

$$\bar{v}_r\frac{\partial \bar{v}_r}{\partial \bar{r}} + \bar{v}_z\frac{\partial \bar{v}_r}{\partial \bar{z}} = -\frac{\partial \bar{p}}{\partial \bar{r}} + \frac{1}{Re}\left\{\frac{\partial}{\partial \bar{r}}\left[\frac{\bar{\mu}}{\bar{r}}\frac{\partial(\bar{r}\bar{v}_r)}{\partial \bar{r}}\right] + \frac{\partial}{\partial \bar{z}}\left[\bar{\mu}\frac{\partial \bar{v}_r}{\partial \bar{z}}\right]\right\} + B\frac{\partial \bar{\psi}}{\partial \bar{r}}\sinh(\bar{\psi}) \tag{17b}$$

$$\bar{v}_r\frac{\partial \overline{T}}{\partial \bar{r}} + \bar{v}_z\frac{\partial \overline{T}}{\partial \bar{z}} = \frac{1}{PrRe}\left\{\frac{1}{\bar{r}}\frac{\partial}{\partial \bar{r}}\left[\bar{r}\bar{k}_l\frac{\partial \overline{T}}{\partial \bar{r}}\right] + \frac{\partial}{\partial \bar{z}}\left[\bar{k}_l\frac{\partial \overline{T}}{\partial \bar{z}}\right]\right\} + \overline{\Phi} + \bar{\dot{q}} \tag{18}$$

$$A = \frac{R\sigma e n_0 E}{\rho U_{\text{ref}}^2/2} \quad B = \frac{n_0 k_b T}{\rho U_{\text{ref}}^2/2}$$
$$\overline{\Phi} = \frac{\Phi}{\rho c_p U_{\text{ref}}(T_0 - T_{\text{ref}})/R} \tag{19}$$
$$\bar{\dot{q}} = \frac{\dot{q}}{\rho c_p U_{\text{ref}}(T_0 - T_{\text{ref}})/R}$$

where A, B are dimensionless parameters, and physically they represent the ratio of the ionic electrostatic energy to kinetic energy and the ratio of the thermal energy to kinetic energy, respectively. The above equations are subject to the following boundary conditions [22]:

At the Inlet, $\bar{z} = 0$

$$T = T_f \quad \bar{\psi} = 0 \quad \frac{\partial \bar{v}_z}{\partial \bar{z}} = 0 \quad \frac{\partial \bar{v}_r}{\partial \bar{z}} = 0 \tag{20a}$$

For the channel length assumed to be sufficiently long, the flow is fully developed at the outlet, $\bar{z} = L/R$, and hence the outlet boundary conditions are

$$\frac{\partial^2 T}{\partial z^2} = 0 \quad \frac{\partial \bar{\psi}}{\partial \bar{z}} = 0 \quad \frac{\partial \bar{v}_z}{\partial \bar{z}} = 0 \quad \frac{\partial \bar{v}_r}{\partial \bar{z}} = 0 \tag{20b}$$

Due to the symmetry, the boundary conditions at the cylinder centerline, $\bar{r} = 0$ are

$$\frac{\partial \overline{T}}{\partial \bar{r}} = 0 \quad \frac{\partial \bar{\psi}}{\partial \bar{r}} = 0 \quad \frac{\partial \bar{v}_z}{\partial \bar{r}} = 0 \quad \bar{v}_r = 0 \tag{20c}$$

At the capillary wall, $\bar{r} = 1$, the following are specified

$$\bar{\psi} = \bar{\zeta} \quad \bar{v}_z = 0 \quad \bar{v}_r = 0 \tag{20d}$$

where $\bar{\zeta}$ is the dimensionless zeta potential defined as $\bar{\zeta} = \sigma e\zeta/k_b T$.

The temperature at the inner capillary wall is unknown. Since the heat generated by Joule heating and viscous dissipation in the electrolyte solution is mainly dissipated through the capillary wall to the surrounding environment, a conjugate heat transfer problem is solved to account for heat conduction in both the solution and the capillary wall [22]. The governing equation for heat conduction in the capillary wall is expressed as

$$\frac{1}{\bar{r}}\frac{\partial}{\partial \bar{r}}\left[\bar{r}\bar{k}_s\frac{\partial \overline{T}}{\partial \bar{r}}\right] + \frac{\partial}{\partial \bar{z}}\left[\bar{k}_s\frac{\partial \overline{T}}{\partial \bar{z}}\right] = 0 \tag{21a}$$

The temperature boundary condition at the channel outside wall is

$$-\bar{k}_s\frac{\partial \overline{T}}{\partial \bar{r}}\bigg|_{\bar{r}=1+\delta/R} = \frac{hR}{k_{\text{ref}}}(\overline{T} - 1) \tag{21b}$$

where δ is the thickness of the capillary wall, $\bar{k}_s$ is dimensionless thermal conductivity of the glass capillary, and h is the heat transfer coefficient outside the capillary.

2.3. Mass species transport equation

So far, the closure governing equations describing the Joule heating and its effect on electroosmotic flow in a microcapillary have been presented. Since electroosmotic flows are often used for injection, delivery and separation of biological or chemical samples, such as the separation of DNA [2], another objective of this work is to study the role of Joule heating in the sample species transport.

Consider a sample species of interest to be transported between two reservoirs in a capillary filled with an electrolyte solution. For analysis, assumptions are made for no adsorption of sample species onto the capillary wall and no interaction between sample species and the electrolyte solution components. As the species transported by electrokinetic means in general is accomplished by three mechanisms including convection, diffusion, and electrophoresis, the mass transport equation can be formulated as [23],

$$\frac{\partial C_i}{\partial t} + (v_z + u_{zi})\frac{\partial C_i}{\partial z} + (v_r + u_{ri})\frac{\partial C_i}{\partial r} = \frac{1}{r}\frac{\partial}{\partial r}\left[rD_i(T)\frac{\partial C_i}{\partial r}\right] + \frac{\partial}{\partial z}\left[D_i(T)\frac{\partial C_i}{\partial z}\right] \tag{22}$$

where C_i is ith sample species concentration, $D_i(T)$ is the temperature-dependent mass diffusivity of the ith sample species, $D_i(T) = D_{i0} + 0.0309D_{i0}(T - 293.13)$ (here D_{i0} is the mass diffusivity of the ith sample species at 293.15 K), and u_{zi} and u_{ri} are the components of the electrophoretic velocity in axial direction and radial direction, respectively. Introducing the following dimensionless parameters:

$$\overline{C}_i = \frac{C}{C_{i\mathrm{ref}}} \quad \bar{t} = \frac{t}{\rho R^2/\mu_{\mathrm{ref}}} \quad \overline{D}_i = \frac{D_i(T)}{D_{i\mathrm{ref}}} \tag{23}$$

Eq. (23) can be non-dimensionalized as

$$\frac{\partial \overline{C}_i}{\partial \bar{t}} + Re(\bar{v}_z + \bar{u}_{zi})\frac{\partial \overline{C}_i}{\partial \bar{z}} + Re(\bar{v}_r + \bar{u}_{ri})\frac{\partial \overline{C}_i}{\partial \bar{r}} = \frac{1}{Sc}\left\{\frac{1}{\bar{r}}\frac{\partial}{\partial \bar{r}}\left[\bar{r}\overline{D}_i\frac{\partial \overline{C}_i}{\partial \bar{r}}\right] + \frac{\partial}{\partial \bar{z}}\left[\overline{D}_i\frac{\partial \overline{C}_i}{\partial \bar{z}}\right]\right\} \tag{24}$$

where $C_{i\mathrm{ref}}$ and $D_{i\mathrm{ref}}$ are respectively the reference concentration and mass diffusivity of the ith species, and $Sc = \frac{\mu_{\mathrm{ref}}/\rho}{D_{i\mathrm{ref}}}$ is the Schmidt number. The initial condition is

$$\bar{t} = 0: \quad \overline{C}_i = 0.0 \tag{25a}$$

The boundary conditions are

$$\begin{aligned} &\text{Inlet:} \quad \bar{z} = 0 \quad \overline{C}_i = 1.0 \\ &\text{Outlet:} \quad \bar{z} = L/R \quad \frac{\partial^2 \overline{C}_i}{\partial \bar{z}^2} = 0 \end{aligned} \tag{25b}$$

$$\begin{aligned} &\text{Centerline:} \quad \bar{r} = 0 \quad \frac{\partial \overline{C}_i}{\partial \bar{r}} = 0 \\ &\text{Capillary wall:} \quad \bar{r} = 1 \quad \frac{\partial \overline{C}_i}{\partial \bar{r}} = 0 \end{aligned} \tag{25c}$$

The numerical scheme used for solving the proposed mathematical models is based on the finite volume method [24]. The above-derived P–B equation, Eq. (6), modified N–S equations, Eqs. (16)–(17), energy equations, Eqs. (18) and (21a), and mass species transport equation, Eq. (24) are discretized using a control volume integration. The non-linear source term in Eq. (6) is linearized using the source term linearization procedure of Patankar [24]. The electroosmotic flow fields are obtained by solving Eqs. (16)–(17) using SIMPLER [24]. To solve the discrete algebraic equations, the line-by-line Tridiagonal Matrix Algorithm (TDMA) scheme is employed. Due to the coupling, Eq. (6) and Eqs. (16)–(18) and (21a) are solved iteratively to obtain the velocity and temperature fields first. The species concentration distribution in the microcapillary described by Eq. (24) is then computed using the converged results of the velocity and temperature fields. A grid independent study indicates that 60×120 control volumes in the radial and axial directions produces grid independent solutions. As such, all results reported in this article are obtained using the above-mentioned grid system.

3. Results and discussion

In this study, the microcapillaries considered are made from silica glass and have a length of $L = 50$ mm and different radii but a fixed wall thickness of $\delta = 70$ μm (e.g., Polymicro Technologies, USA). The working fluid is NaCl solution and its properties are: density $\rho = 998$ kg/m^3, electric conductivity (at room temperature 20 °C) $\lambda_{+0} = 50.08 \times 10^{-4}$ m^2 S/mol and $\lambda_{-0} = 76.31 \times 10^{-4}$ m^2 S/mol [25]. DNA species is chosen as the sample transport in the microcapillary, and its mass diffusivity and electrophoretic mobility (at 20 °C) are $D_{i0} = 2.03 \times 10^{-11}$ m^2/s and $u_{zi0} = u_{ri0} = 2.74 \times 10^{-8}$ m^2/V s, respectively [26]. Parametric studies including capillary radius, solution concentration and zeta potential, applied electric field strength, and heat transfer coefficient are carried out to quantitatively examine the Joule heating effect on the electroosmotic flow and mass species transport.

3.1. Effect of the capillary size

The radial temperature distributions (in the thermal fully developed regime) in the liquid solution and the solid capillary wall for three different capillary radii are shown in Fig. 2a. It is seen that the temperature distributions in the liquid exhibit a parabolic-like pattern, supporting the assumptions made by Grushka and coauthors [17,18]. This also shows that the heating due to viscous dissipation is not important. However, the parabolic shape seems to vary from case to case, depending parametric conditions. The highest temperature occurs at the capillary centerline, suggesting that the heat generated by Joule heating is transferred from the central region to the wall by convection, and then dissipated through the capillary wall by conduction. Further, under the same physicochemical conditions, $E = 500$ V/cm, $C = 0.1$ M, $\zeta = -50$ mV, and $h = 10$ W/m^2 K, the temperatures of both the liquid solution and solid wall in a large capillary ($R = 200$ μm) are significantly higher than those in a small capillary ($R = 50$ μm). The same trend can also be observed in the plots of the axial bulk temperature profile of the liquid solution in capillaries shown in Fig. 2b. The scenario may be attributed to the fact that as the capillary size becomes larger, the surface area-to-volume ratio becomes smaller, leading to a lower ratio of the heat dissipation (measured by surface) to the Joule heat generation (defined by volume). However, from a practical design viewpoint, choice of small-sized capillaries may be problematic because the sample species adsorption is enhanced for small capillaries the detection sensitivity will decrease and.

In addition, according to Yang et al. [11], the hydrodynamic entrance length of electroosmotic flows is negligible due to very low Reynolds numbers. In the present study, the typical Reynolds number is about

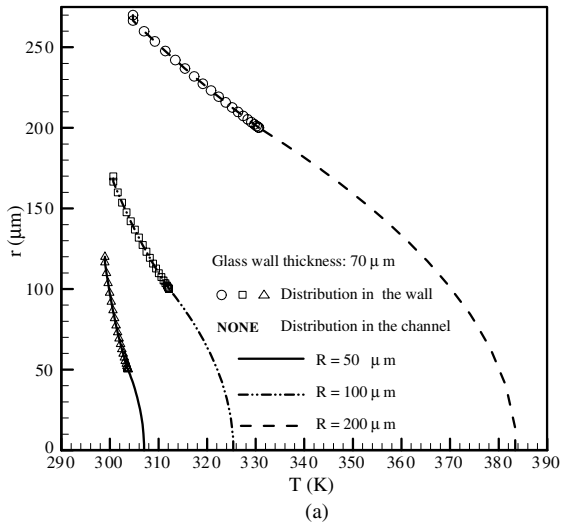

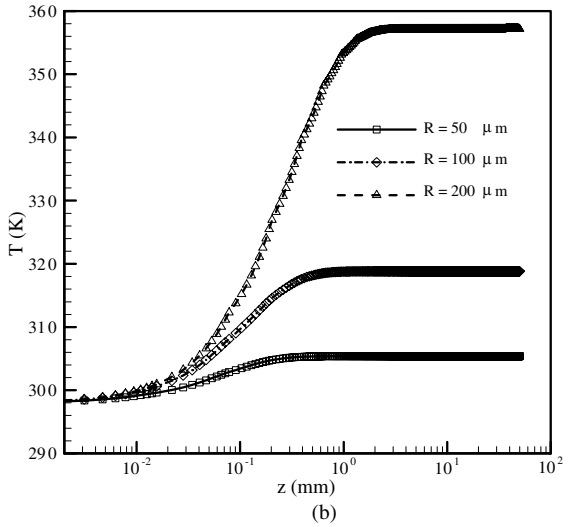

Fig. 2. Temperature distributions in the capillary and its solid wall for various capillary radii: (a) radial temperature distribution and (b) axial solution bulk temperature profile.

$Re = 0.01$, giving rise to the entrance regime of the hydrodynamic flow of about 1% of the capillary radius only [11]. However, the thermal entrance due to Joule heating in electroosmotic flow is quite significant (see Fig. 2b). The thermal entrance length is approximately about ten times as large as the capillary radius.

Fig. 3 shows the dimensionless fully developed electroosmotic flow velocity distributions for three different capillary radii. In all computations, the reference velocity is defined as $U_{\text{ref}} = (\varepsilon_{\text{ref}}\varepsilon_0/\mu_{\text{ref}})E\zeta$ unless specified otherwise. In the absence of Joule heating, the velocity profile is uniform throughout most of the capillary. The unity dimensionless velocity indicates that the maximum velocity is determined by the Smoluchowski

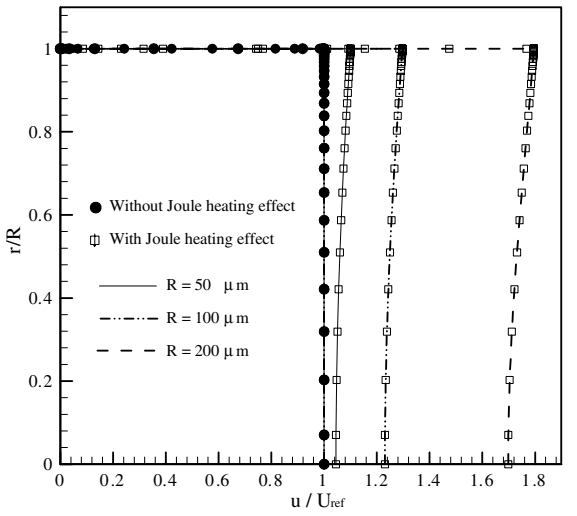

Fig. 3. Solution radial velocity distributions with/without Joule heating effects for various capillary radii.

velocity [1], $U_s = \varepsilon\varepsilon_0 E\zeta/\mu$, and is independent of the capillary radius. While in the presence of Joule heating, as previously discussed, the fluid temperature increases with capillary size. This leads to lower liquid viscosity which in turn results in higher fluid velocity as shown in Fig. 3. It is also observed that the velocity reaches a maximum value near the capillary wall. This is expected because the driving force in an electroosmotic flow is due to the interplay between the applied electric field and the net electric charge density that only exists within the thin EDL regime close to the wall. The flow extended to the rest region of the capillary is passive, and is attributed to hydrodynamic shear stresses due to viscosity.

Variation of the sample mean concentration along the axial direction for different capillary radii (at a specific time of $t = 10$ s) and evolution of the sample species concentration distributions in a capillary are shown in Figs. 4 and 5, respectively. Because of the low diffusion coefficient of sample species (for DNA, $D_i = 10^{-11}$ m^2/s [26]), we can estimate the order of the Peclet number, $Pe = \bar{u}R/D_i$ is of $O(10^2)$, suggesting that the species transport is dominated by convection and mainly transported with the flow. Under the case of no Joule heating effect, it is noted that the sample concentration transport is independent of the capillary size (see Fig. 4) and exhibits non-dispersive (see Fig. 5); these are unique advantages used in the BioMEMS design [3]. In the presence of Joule heating, it is noted from Fig. 4 that the sample species transports much faster in larger capillaries due to an increase of the electroosmotic velocity (see Fig. 3). In addition, since the sample electrophoresis mobility increases with increasing temperature, the presence of radial temperature gradient gives rise to a

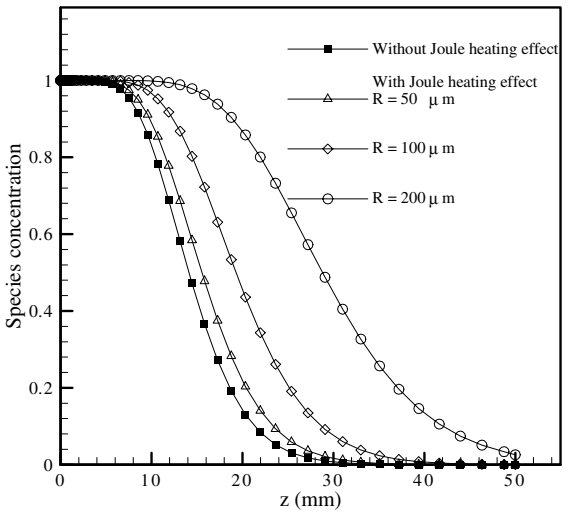

Fig. 4. Variation of sample mean concentration along the axial direction with/without Joule heating effects for various capillary radii at the time $t = 10$ s.

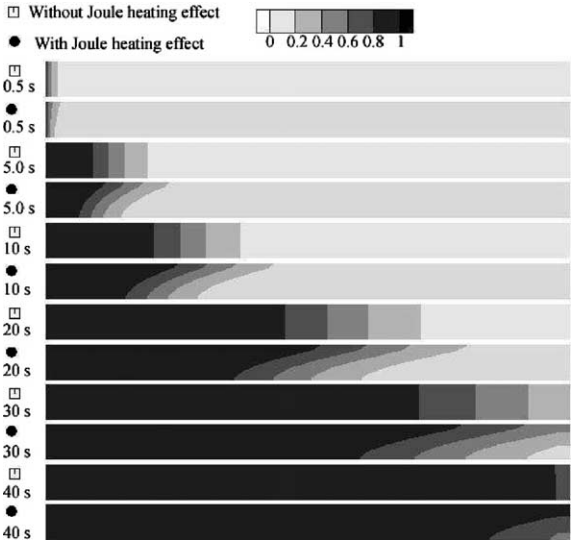

Fig. 5. Evolution of species concentration distributions in the capillary of $R = 100$ μm at different time without/with Joule heating effects.

variation of the sample axial electrophoresis mobility along the radial direction, and hence results in the sample species very dispersive. While the direction of the electrophoresis velocity for negatively charged samples (e.g., DNA species) is opposite to electroosmosis velocity, we can clearly observe from Fig. 5 that the sample species in the central region transports much slower than that close to the wall region, and such difference gets larger as time elapses. This finding suggests that as the Joule heating is concerned, the dispersive effect needs to be considered in the BioMEMS design.

3.2. Effect of the solution concentration

Fig. 6a and b present the radial temperature distributions and the axial bulk temperature profile in a capillary for three different solution concentrations, respectively. It is well-known that the capillary zeta potential is correlated to the solution concentration [21]. Hence, a variation of the zeta potentials is also included, and they are $C = 10^{-4}$ M ($\zeta = -150$ mV), $C = 10^{-2}$ M

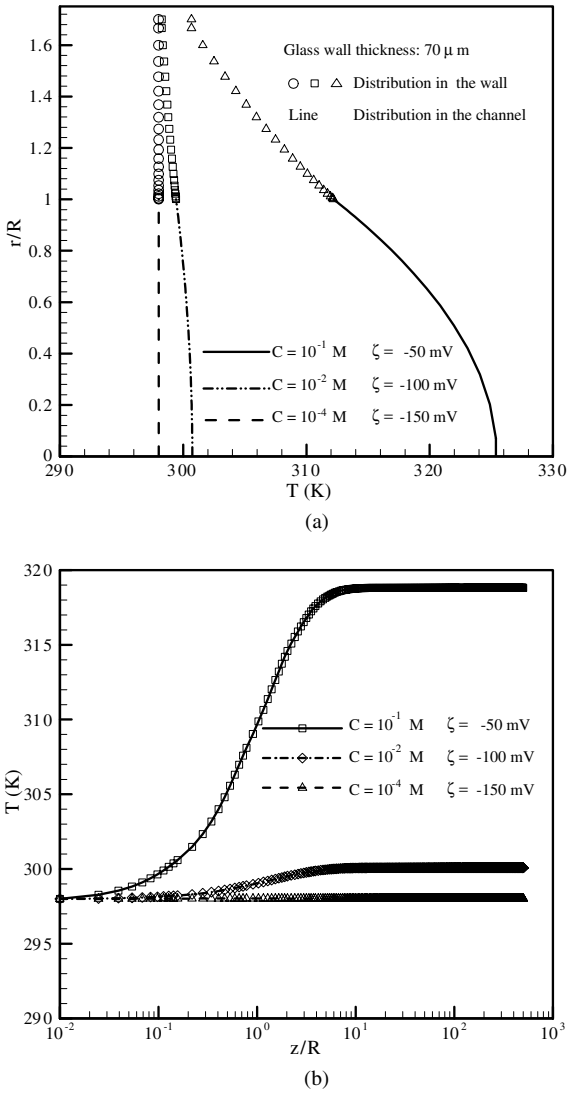

Fig. 6. Temperature distributions in the capillary and its solid wall for various combinations of the solution concentration and zeta potential: (a) radial temperature distribution and (b) axial solution bulk temperature profile.

($\zeta = -100$ mV), and $C = 10^{-1}$ M ($\zeta = -50$ mV). Other parameters are: $R = 100$ μm, $E = 500$ V/cm, and $h = 10$ W/m^2 K. According to Eq. (14), the heat generation due to Joule heating $\dot{q} = (v_z\rho_e + E\lambda)^2/\lambda$ is associated with the liquid electrical conductivity, λ, which in turn depends on the solution concentration. Hence, as expected, the solution temperature rise increases with increasing solution concentration. This indicates that the Joule heating can be safely neglected for dilute electrolytes (e.g., $C = 10^{-4}$ M). However, for an electrolyte of high concentrations (e.g., $C = 10^{-1}$ M), the Joule heating effect under parameters studies can lead to a 20 °C temperature increment, which has an impact on the electroosmotic flow velocity distributions (shown in Fig. 7) and the variation of the mean sample species concentration along the axial direction (shown in Fig. 8). From Fig. 7, it can be seen that, due to large values of the electrokinetic radius, κR, the solution concentration itself has negligible effects on the dimensionless velocity distributions. However, as can be predicted from the Smoluchowski equation [1], $U_s = [\varepsilon(T)\varepsilon_0/\mu(T)]E\zeta$, the magnitude of the velocity is proportional to the zeta potential, which is related to the solution concentration as mentioned earlier. This is clearly demonstrated in Fig. 8 that the sample species moves much further into the capillary as the high zeta potential increases. In addition, according to Eq. (14), $\dot{q} = (v_z\rho_e + E\lambda)^2/\lambda$, the Joule heating consists of two contributions: the first is due to the convection electric current, $v_z\rho_e$, and the second is related to the conduction electric current, $E\lambda$. Based on the EDL theory, the electric net charge density, ρ_e which is mainly determined by the zeta potential, only exists within the thin EDL regime close to the capillary wall. In other words, in the majority portion of the capillary (larger than 98%), ρ_e is nearly zero. Thus, as indicated in Fig. 8, the results show both the electroosmotic flow velocity and zeta potential have insignificant effects on Joule heating. The major contribution to Joule heating is due to the conduction current, $E\lambda$, which, in turn, is related to the solution concentration.

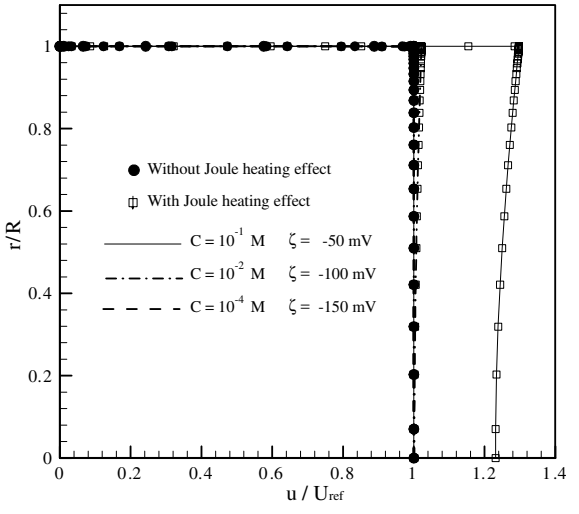

Fig. 7. Solution radial velocity distributions with/without Joule heating effects for various combinations of the solution concentration and zeta potential.

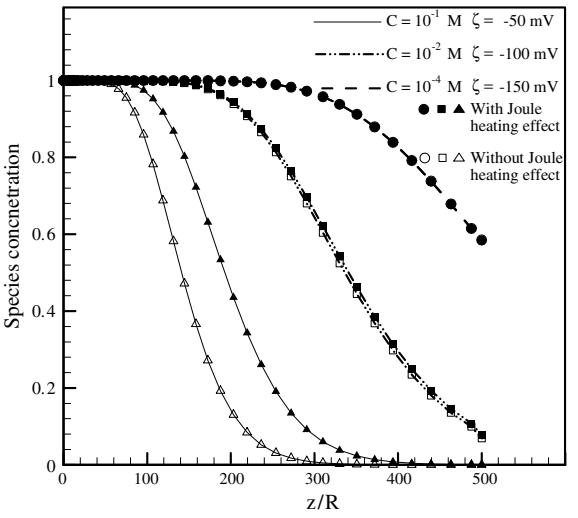

Fig. 8. Variation of sample mean concentration along the axial direction with/without Joule heating effects for various combinations of the solution concentration and zeta potential at the time $t = 10$ s.

3.3. Effect of the applied electric field

As discussed earlier, the contribution to Joule heating due to the convection electric current, $v_z\rho_e$ is minor. If neglecting $v_z\rho_e$, we can simplify Eq. (14) to $\dot{q} \approx E^2\lambda$, suggesting the Joule heating would strongly depend on the applied electric field strength, E. The quantitative supporting evidences are shown using the radial temperature distributions (Fig. 9a) and the axial mean temperature profile (Fig. 9b) in a capillary for three different electric field strengths. Other parameters used in calculations are: $R = 100$ μm, $C = 0.1$ M, $\zeta = -50$ mV, and $h = 10$ W/m^2 K. The results in Fig. 9a and b show that for parameters considered, the Joule heating effect under low field strength is negligible (e.g., $E = 100$ V/cm). Under high electric field strength, for instance $E = 1000$ V/cm, the present single-phase model predicts that the solution temperature can increase up to above 100 °C, and hence vapor bubbles could be generated. The experimental evidence of the presence of vapor bubbles under high electric fields was reported in the literature. Figs. 10 and 11 respectively show the effects of applied electric field on electroosmotic flow velocity

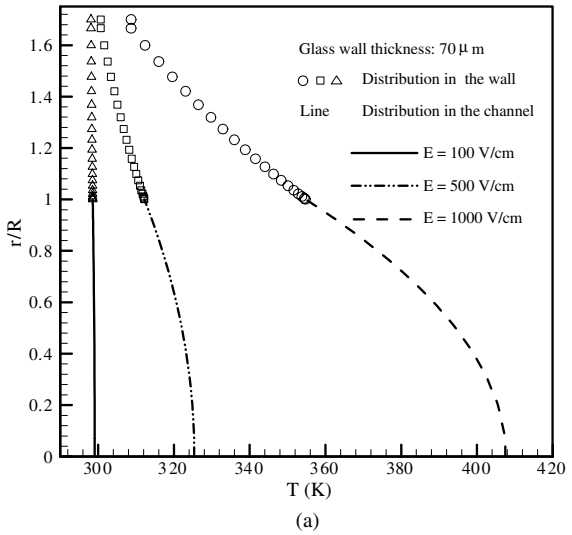

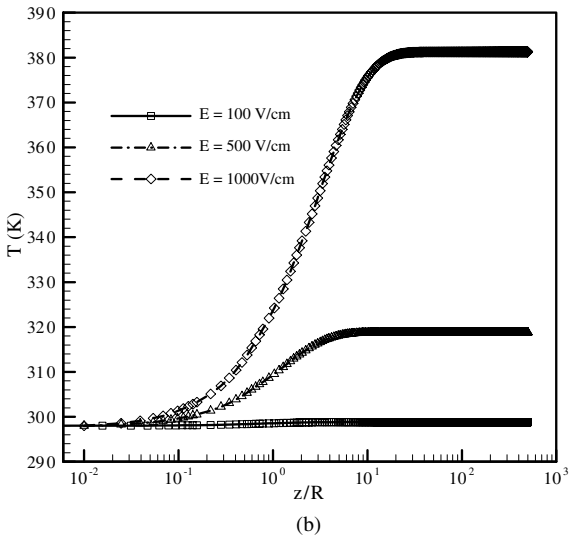

Fig. 9. Temperature distributions in the capillary and its solid wall for various applied electric field strengths: (a) radial temperature distribution and (b) axial solution bulk temperature profile.

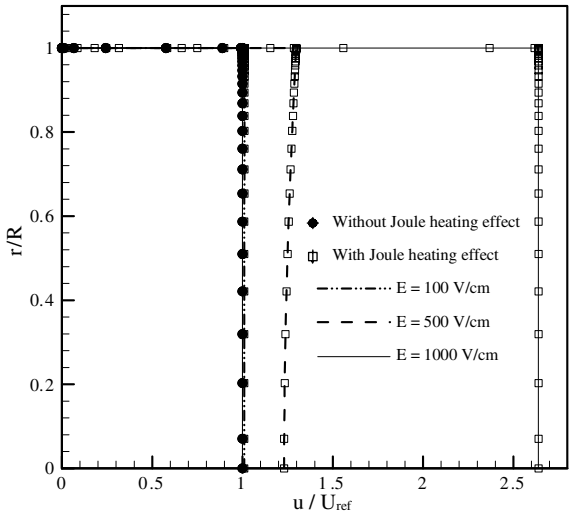

Fig. 10. Solution radial velocity distributions with/without Joule heating effects for various applied electric field strengths.

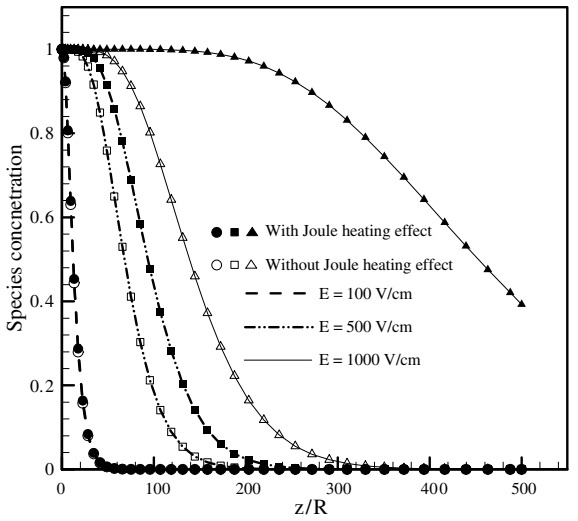

Fig. 11. Variation of sample mean concentration along the axial direction with/without Joule heating effects for various applied electric field strengths at the time $t = 10$ s.

distributions and the variation of the mean sample species concentration along the axial direction with and without consideration of the Joule heating. Similar to the capillary radius and zeta potential, a change of the field strength does not affect the non-dimensional velocity distribution if the Joule heating is not included. In the presence of Joule heating, a temperature increment causes the velocity distribution to deviate from the normal situation. It is interesting to find that under the highest electric field considered in this study, the velocity distribution at the central region does not show any depression as those observed in Figs. 3 and 7. A possible explanation is that the high electric field can result in very strong driving forces for the electroosmotic flow. It seems further studies are needed in future to confirm this argument.

3.4. Effect of the heat transfer coefficient

In most commercial CE systems, the cooling systems are required to ensure effective heat removal. Therefore

the effect of the heat transfer coefficient outside the capillary wall is investigated. Three different heat transfer coefficients namely: 1, 10 and 100 W/m^2 K, are considered. These correspond to the nature convective cooling system, air forced-convection system and liquid forced-convection system, respectively. Other parameters used in calculations are: $R = 100$ μm, $E = 500$ V/cm, $C = 0.1$ M, and $\zeta = -50$ mV. The calculated radial temperature distributions and the axial bulk temperature profiles in a capillary under the influence of the heat transfer coefficient are presented in Fig. 12a and b, respectively. Interestingly, the shape of radial temperature distributions is almost the same, irrespective of different heat transfer coefficients. Figs. 13 and 14 show the electroosmotic flow velocity distributions and the variation of the mean sample species concentration along the axial direction, respectively. The results demonstrate that the choice of cooling system has a strong impact on the electroosmotic flow velocity and sample transport in microcapillaries.

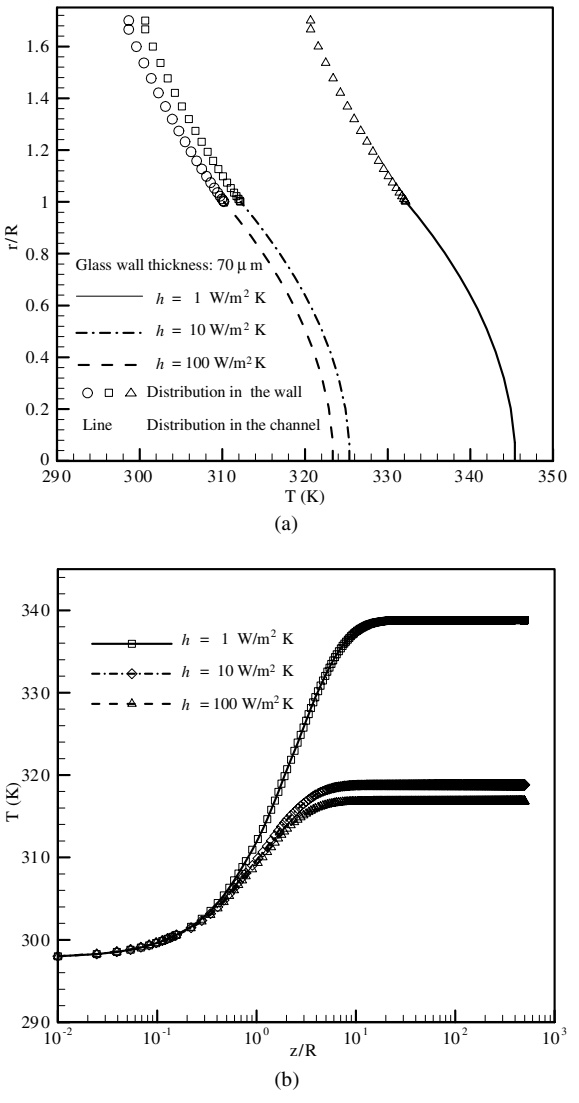

Fig. 12. Temperature distributions in the capillary and its solid wall under the influence of the heat transfer coefficient outside the capillary wall: (a) radial temperature distribution and (b) axial solution bulk temperature profile.

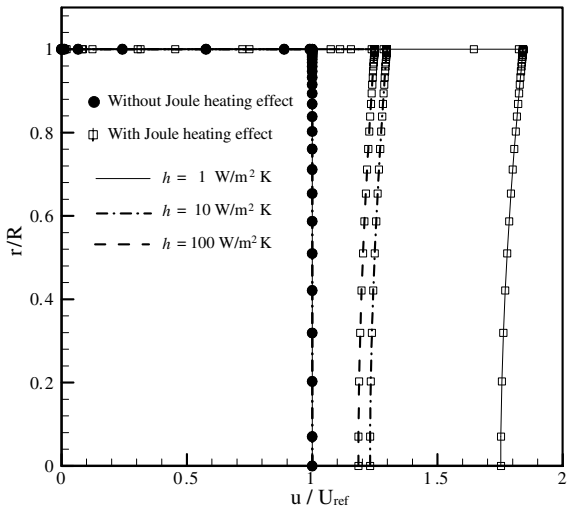

Fig. 13. Solution radial velocity distributions in a microcapillary under the influence of the heat transfer coefficient outside the capillary wall.

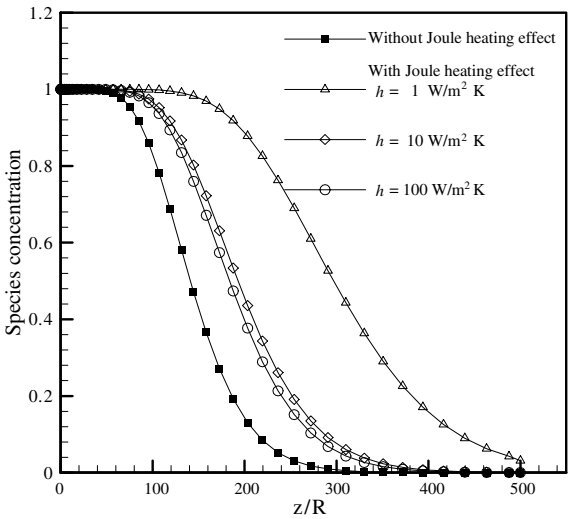

Fig. 14. Variation of sample mean concentration along the axial direction under the influence of the heat transfer coefficient outside the capillary wall at the time $t = 10$ s.

4. Concluding remarks

A rigorous mathematic model for describing the effect of Joule heating on the electroosmotic flow and sample species electrokinetic transport in microcapillaries is developed. The proposed model includes the P–B equation for the EDL field, the N–S equations for electroosmotic flow velocities, the conjugate energy equation for temperature distributions in both liquid solution and solid capillary wall, and the electrokinetic transport equation for sample species concentration distributions. Thermophyscial properties including the solution dielectric constant, viscosity, and thermal conductivity and sample species mass diffusivity and electrophoretic mobility are considered to be temperature-dependent. The aforementioned equations are numerical solved using a finite-volume-based CFD technique.

The simulations demonstrate that the presence of Joule heating could have a great impact on the electroosmotic flow and sample species transport. It is found that the Joule heating effect is significant for large-sized capillaries, concentrated buffer solutions, high externally applied electric field strengths, and poor cooling modes outside the capillary. The results show that the Joule heating causes the development of both radial and axial temperature distributions in the capillary. The temperature increment and the presence of temperature gradients could lead to a deviation of the electroosmotic flow velocity from its normal profile, and also make the sample species axially transport faster and more dispersive along the radial direction of the capillary. In addition, the calculations reveal that compared to the conduction current, the contribution to the Joule heating due to convection current is negligible under the parameters studied. Future studies will include development of an experimental setup to verify the simulation results, which is in process now.

Acknowledgements

The authors would like to gratefully acknowledge the financial support of the Academic Research Fund (RG07/02) to CY and the Ph.D. scholarship awarded to GYT from the Nanyang Technological University.

References

[1] R.F. Probstein, Physicochemical Hydrodynamics: An Introduction, second ed., John Wiley and Sons, New York, 1994.
[2] D.J. Harrison, K. Fluri, K. Seiler, Z. Fan, C.S. Effenhauser, A. Manz, Micromachining a miniaturized capillary electrophoresis-based chemical analysis system on a chip, Science 261 (1993) 895–897.
[3] L. Bousse, C. Cohen, T. Nikiforov, A. Chow, A.R. Kopf-Sill, R. Dubrow, J.W. Parce, Eelectrokinetically controlled microfluidic analysis systems, Annu. Rev. Biophys. Biomol. Struct. 29 (2000) 155–181.
[4] D. Burgreen, F.R. Nakache, Electrokinetic flow in ultrafine capillary slits, J. Phys. Chem. 68 (1964) 1084–1091.
[5] C.L. Rice, R. Whitehead, Electrokinetic flow in narrow cylindrical capillaries, J. Phys. Chem. 69 (1965) 4017–4023.
[6] Y.J. Kang, C. Yang, X.Y. Huang, Dynamic aspects of electroosmotic flow in a cylindrical microcapillary, Int. J. Eng. Sci. 40 (2002) 2203–2221.
[7] Y.J. Kang, C. Yang, X.Y. Huang, Electroosmotic flow in a capillary annulus with high zeta potentials, J. Colloid Interface Sci. 253 (2002) 285–294.
[8] J.P. Hsu, C.Y. Kao, S. Tseng, C.J. Chen, Electrokinetic flow through an elliptical microchannel: effects of aspect ratio and electrical boundary conditions, J. Colloid Interface Sci. 248 (2002) 176–184.
[9] C. Yang, D. Li, Electrokinetic effects on pressure-driven liquid flows in rectangular microchannels, J. Colloid Interface Sci. 194 (1997) 95–107.
[10] N.A. Patankar, H.H. Hu, Numerical simulation of electroosmotic flow, Anal. Chem. 70 (1998) 1870–1881.
[11] R.J. Yang, L.M. Fu, C.C. Hwang, Electroosmotic entry flow in a microchannel, J. Colloid Interface Sci. 244 (2001) 173–179.
[12] J.G. Santiago, Electroosmotic flows in microchannels with finite inertial and pressure forces, Anal. Chem. 73 (2001) 2353–2365.
[13] J.H. Knox, K.A. McCormack, Temperature effects in capillary electrophoresis. 1. Internal capillary temperature and effect upon performance, Chromatographia 38 (1994) 207–214.
[14] J.H. Knox, K.A. McCormack, Temperature effects in capillary electrophoresis. 2. Some theoretical calculations and predictions, Chromatographia 38 (1994) 215–221.
[15] E. Grushka, R.M. McCormick, J.J. Kirkland, Effect of temperature gradients on the efficiency of capillary zone electrophoresis separations, Anal. Chem. 61 (1989) 241–246.
[16] A.E. Jones, E. Grushka, Nature of temperature gradient in capillary zone electrophoresis, J. Chromatogr. 466 (1989) 219–225.
[17] M.A. Bosse, P. Arce, The role of Joule heating in dispersive mixing effects in electrophoretic cells: hydrodynamic considerations, Electrophoresis 21 (2000) 1018–1025.
[18] M.A. Bosse, P. Arce, Role of Joule heating in dispersive mixing effects in electrophoretic cells: convective-diffusive transport aspects, Electrophoresis 21 (2000) 1026–1033.
[19] K. Swinney, D.J. Bornhop, Quantification and evaluation of Joule heating in on-chip capillary electrophoresis, Electrophoresis 23 (2002) 613–620.
[20] W.A. Gobie, C.F. Ivory, Thermal model of capillary electrophoresis and a method for counteracting thermal band broadening, J. Chromatogr. 516 (1990) 191–210.
[21] R.J. Hunter, Zeta Potential in Colloid Science: Principles and Applications, Academic Press, New York, 1981.
[22] C. Yang, D. Li, J.H. Masliyah, Modeling forced liquid convection in rectangular microchannels with electrokinetic effects, Int. J. Heat Mass Transfer 41 (1998) 4229–4249.

[23] S.V. Ermakov, S.C. Jacobson, J.M. Ramsey, Computer simulations of electrokinetic transport in microfabricated channel structures, Anal. Chem. 70 (1998) 4494–4504.
[24] S.V. Patankar, Numerical Heat Transfer and Fluid Flow, McGraw-Hill, New York, 1980.
[25] R. Weast, M.J. Astle, W.H. Beyer, CRC Handbook of Chemistry and Physics, CRC Press Inc., Boca Raton, 1986.
[26] T. Ohara, D. Torii, A. Majumdar, K. Dunphy, Transport of biomolecules in the ratcheting electrophoresis microchip (REM), in: The Sixth ASME-JSME Thermal Engineering Joint Conference, 2003, TED-AJ03-406.